*Int. J. Electrochem. Sci.*, 7 **(2012)** 7404 - 7424

International Journal of
ELECTROCHEMICAL
SCIENCE
www.electrochemsci.org

# Characterization of the Localized Surface Chemical Activity of Ti-Mo and Ti-Ta Alloys for Biomedical Applications Using Scanning Electrochemical Microscopy

*G. Ciurescu*[1,2], *J. Izquierdo*[1], *J.J. Santana*[1,3], *D. Mareci*[2], *D. Sutiman*[2], *S. González*[1], *R.M. Souto*[1,*]

[1] Department of Physical Chemistry, University of La Laguna, E-38205 La Laguna (Tenerife, Canary Islands), Spain
[2] Faculty of Chemical Engineering and Environmental Protection, ''Gh.Asachi'' Technical University of Iasi, B-dul D. Mangeron, nr. 59, 700050 Iasi (Romania)
[3] Department of Process Engineering, University of Las Palmas de Gran Canaria, Campus Universitario de Tafira, E-35017 Las Palmas de Gran Canaria (Gran Canaria, Canary Islands), Spain.
[*]E-mail: rsouto@ull.es

*Received:* 3 July 2012 / *Accepted:* 20 July 2012 / *Published:* 1 August 2012

Scanning electrochemical microscopy (SECM) was employed for *in situ* characterization of surface chemical activity of various Ti-Mo and Ti-Ta alloys for biomedical application. In this work the local differences in surface reactivity for different Ti-Mo and Ti-Ta alloys were analyzed when they were polarized in 0.1 M NaCl solution and in Ringer's physiological solution using SECM, and results compared to those for the unbiased samples. The analysis of the shape of the approach curves obtained for the Ti-Mo and Ti-Ta alloys shows a different behaviour to be distinguished depending on the nature of the alloying element. There are also differences among the various Ti-Ta alloys tested, that cause changes in the shape of the approach curves with the value of the polarization applied to the substrate, defining a transition potential between -0.30 and -0.40 V vs. Ag/AgCl/KCl(3M) for most of the systems under study. Furthermore, from the line scans and array scans, a change in reactivity of the surface has been observed corresponding to the activation of the localized sites which occurs selectively with the applied potential. SECM is shown to be a powerful technique for the investigation of the surface characteristics of biomaterials in simulated physiological environments.

**Keywords:** Scanning electrochemical microscopy; Ti-Ta alloys; surface chemical activity; passivity.

## 1. INTRODUCTION

Titanium and titanium-based alloys are very widely employed in biomedical applications due to their low elasticity modulus, high corrosion resistance and excellent biocompatibility [1,2]. Compact and stable oxide layers are formed on these materials because of their state of passivity in

physiological environments [3]. The actual composition of the passive film is still rather controversial, but most investigators agree that the film consists of titanium dioxide, $TiO_2$. Though pure titanium and Ti-6Al-4V are the major materials for manufacture of orthopaedic implants, the poor shear strength of these materials has effectively led to restrict their effective service life to 10-15 years. This has stimulated material scientists to develop titanium alloys with lower mechanical modulus, thus closer to bone, and to explore them as for biocompatibility and corrosion resistance [4,5]. Additionally, candidate biomaterials exhibiting non-toxic and non-allergenic properties [6,7] are titanium alloys containing β-stabilizing elements. In this way, alloys containing Nb [7-10], Ta [11-19], Mo [8,10,20-24], Hf [16,25], Zr [26], and combinations of these elements [27-33] are investigated. Among them, tantalum is an element that is widely used today in different areas of medicine, due to its high corrosion resistance and good behaviour as a biomaterial, being regarded to present one of the highest biocompatibilities in the human body [13,34].

Some investigations have examined the biocompatibility of Ti-5Ta [35], Ti-40Ta and Ti-50Ta type alloys [13]. Unlike Ti, which is severely attacked under reducing acids, except when the media contains oxidizing species, such as oxygen, ferric ion, cupric ion and chromic ion, tantalum has an excellent corrosion resistance in neutral environments, oxidizing and reducing acids, and in the presence of hydrofluoric acid [36]. This high corrosion resistance is due to the formation of a tantalum pentoxide layer, $Ta_2O_5$. Therefore, Ti-Ta alloys have benefits when they are used in reducing acid media, having a lower cost and density than Ta, and a greater corrosion resistance compared with Ti [37]. However, scarce studies regarding the corrosion resistance and the electrochemical behaviour of Ti-Ta alloys in aqueous media are available until now [13,37-39], and they rely on the application of conventional electrochemical techniques that average all the surface such as polarization measurements [13,17,19,37-39] and electrochemical impedance [17,19,37]. Nevertheless, spatially-resolved *in situ* investigation of corrosion resistance and chemical reactivity in titanium and its alloys at micrometric and sub-micrometric scale has become possible with the advent of the scanning electrochemical microscope (SECM) [40-43]. Indeed, this technique has already been employed to detect precursor sites for localized pitting corrosion on passivated titanium [44-46], and its ability to *in situ* image electron transfer reactions at metal-metal oxide surfaces [47,48], particularly in the case of thin films of $TiO_2$ and $Ta_2O_5$ [47-50], has recently opened the way to analyze the effect of alloying elements and impurities on the localized reactivity of titanium alloys [51]. The surface layers formed on these materials may vary in thickness from a few molecules to microns, producing major changes in their chemical behavior, chemical composition, crystallinity and electronic properties. Heterogeneities and defects in these layers usually pass undetected using either conventional electrochemical or surface analysis techniques, but small variations in the thickness of insulating oxide layers are sufficient to produce variations in the mechanism of electron transfer kinetics at those surfaces [52,53]. Additionally, local defects may lead to a mechanistic change from electron transfer to ion dissolution at those sites [54-56]. Scanning electrochemical microscopy allows such changes to be detected, as well as variations in the properties of the thin oxide layer with electric potential to be monitored.

The aim of this study was to characterize the corrosion resistance of various Ti-Ta alloys compared to the Ti-20Mo alloy in simulated physiological solutions under different electrical conditioning of the samples, in order to characterize any differences in surface reactivity. In this case, maps of the chemical activity of the oxide layer/electrolyte solution interface related to small active sites on their surfaces could be obtained by SECM. The electrical state of the material was carefully checked, either by letting it at its spontaneously-developed open circuit potential in the simulated physiological environment, or by applying polarization control. Thus, the corrosion resistance of the tested materials could be established from *in situ* measurements with high spatial resolution.

## 2. EXPERIMENTAL

### *2.1. Materials*

Four titanium alloys with the compositions shown in Table 1 were investigated. They consisted of circular rods of 5000 μm approximate diameter inserted in a Teflon insulating matrix. These samples were mechanically ground with SiC abrasive paper with grit from 500 to 1200, and then polished with 3 and 0.5 microns alumina suspension. They were washed with deionised water and left to dry at room temperature for about 2 hours.

**Table 1.** Chemical composition (%wt.) of Ti-Ta and Ti-Mo alloys

| Alloy/Element | Ta | O | Mo | Fe | C | N | Ti |
|---|---|---|---|---|---|---|---|
| Ti-20Mo | - | 0.15 | 20.2 | 0.13 | 0.021 | 0.014 | balance |
| Ti-30Ta | 29.5 | 0.15 | - | 0.13 | 0.021 | 0.015 | balance |
| Ti-40Ta | 39.3 | 0.14 | - | 0.13 | 0.019 | 0.014 | balance |
| Ti-50Ta | 48.9 | 0.14 | - | 0.12 | 0.019 | 0.014 | balance |

The tests were carried out in 0.1 M NaCl solution and in Ringer's physiological solution with pH = 6.4. Experiments were performed at room temperature (about 20 °C) and the solutions were naturally aerated. Ferrocene–methanol of concentration 0.5 mM was added to the test electrolyte solutions to act as electrochemical mediator at the SECM tip. All solutions were prepared with analytical grade reagents and ultra-pure water purified with a Milli-Q system from Millipore.

### *2.2. Instruments*

Experiments were carried out by using a CH900 scanning electrochemical microscope (CH Instruments, Austin, TX, USA), controlled with a personal computer. The electrochemical cell was equipped with a 10 μm platinum microelectrode as the probe, an Ag/AgCl/KCl(3M) as reference

electrode and a Pt wire as counter electrode, all set up in a cell made of polytetrafluoroethene. Specimens were mounted horizontally facing upwards. The cell was located inside a Faraday cage. Specimens were used either unbiased at their open-circuit corrosion potential, or under potentiostatic polarization using the bipotentiostat associated with the SECM. When the specimen was polarised an electrical contact was made through the back of the cell, and potential values in the $0 \geq E \geq -0.70$ V vs. Ag/AgCl/KCl(3M) were applied. The micromanipulator stand of the SECM instrument was used to hold the microelectrode in place.

The sample was located at the bottom of a small flat cell [57], thus exposing one side upwards to the test solution. When the cell and all peripherals were mounted in position, and the imposed experimental parameters had been set, the appropriate electrolyte was inserted into the cell and the microelectrode tip scanned over the surface. The establishment of the operating tip distance over the sample was performed, by recording the corresponding approach curve of the electrochemical mediator. The tip sample was placed over a portion of the surface of the surrounding Teflon mount, using this insulating substrate to produce a negative feedback effect on the faradaic current measured at the microelectrode due to the constraints for diffusion imposed by the proximity of the insulating sample. A 75% negative feedback effect recorded in the tip current was used to establish the reference distance for the *z*-axis. Subsequently, the tip was withdrawn 10 μm from the sample surface, and the positioning motors were employed to move the tip parallel to the surface until reaching the centre of the titanium alloy. Scans were conducted both vertically (*z*-approach curves) and parallel to the sample surface. In the later, the measurements were performed with the microelectrode at a constant height of 10 μm over the titanium alloy surface.

### *2.3. Experimental procedures*

SECM operated in the feedback mode has been employed to investigate the surface reactivity of titanium alloys immersed in simulated physiological solutions. The test environments were 0.1 M NaCl as model system, and Ringer's physiological solution. In the measurements an electrochemical mediator, ferrocene-methanol, was added to both test solutions, and the tip potential was set at +0.50 V vs. Ag/AgCl/KCl(3M) to follow the oxidation of ferrocene-methanol to ferrocinium ion [58]. The choice of this organic compound has been based on previous reports [51,59] that showed ferrocene-methanol to be a suitable redox mediator for the investigation of titanium alloy surfaces. The SECM tip is made the working electrode for the diffusion-limited oxidation of the mediator species *A*, and the corresponding current, $i_{T,\infty}$, for a disk-shaped microelectrode when it is far from any surface, is given by [60]:

$$i_{T,\infty} = 4\, n\, F\, D_A\, C_A^{*}\, a \qquad (1)$$

where $D_A$ and $C_A^*$ are respectively the diffusion coefficient and the bulk concentration of the species *A* in the electrolyte solution, *n* is the number of electrons exchanged in the redox reaction, and *a* is the tip radius. The SECM response is based on how the current of this microelectrode is perturbed by the presence of a substrate near the tip [61].

**Table 2.** Open circuit potential values spontaneously developed by the Ti-Mo and Ti-Ta alloys immersed in the given test solutions.

| | $E_{ocp}$ / V vs. Ag/AgCl/KCl(3M) | |
|---|---|---|
| | 0.1 M NaCl | Ringer's solution |
| Ti-20Mo | -0.040 | -0.127 |
| Ti-30Ta | -0.386 | -0.116 |
| Ti-40Ta | -0.414 | -0.310 |
| Ti-50Ta | -0.085 | -0.132 |

When the tip approaches an inert non-conductive sample, the current will be smaller than $i_{T,\infty}$, because the surface blocks the diffusive flux of *A* to the tip. In the *z*-approach curve towards the surface, the tip current will steadily diminish as the tip gets closer to the insulator surface, eventually becoming zero when the microelectrode touches the sample (negative-feedback behaviour). Conversely, for an active conductive surface, regeneration of the redox mediator occurs at the substrate and thus the tip current will steadily increase as the tip gets closer to the active surface, eventually becoming infinite when the microelectrode touches the sample (positive-feedback behaviour).

Two different measuring procedures have been performed to demonstrate the application possibilities of the SECM technique for the *in situ* investigation of the corrosion resistance of titanium alloys, namely:

- In a first procedure, *z*-approach curves were measured above the titanium alloy samples to explore the eventual blocking of surface films towards the conversion of the redox mediator, and their *insulating characteristics* towards charge transfer reactions. The *z*-approach curves are obtained when the SECM-microelectrode is moved towards the surface in a controlled motion, with the result of variations in the signal measured at the tip due to the near-field effect originating in the proximity of the sample. The potential of the tip is set at +0.50 V vs. Ag/AgCl/KCl(3M) to attain the diffusion-controlled oxidation of ferrocene–methanol to ferrocinium. The samples were either left unbiased, that is, at their open-circuit potential value in the environment, or polarised in the $0 \geq E \geq -0.70$ V vs. Ag/AgCl/KCl(3M) potential range. For the sake of normalization, the dimensionless tip current, $i/i_{lim}$, was employed throughout.

- In a second procedure, the SECM-tip has been scanned parallel to the surface to detect *local variations in chemical reactivity* in the alloys which may be the onset sites for corrosion processes. Local features at the surface of the substrate cause changes in the current response at the SECM-tip when scanned at a constant distance, 10 μm, above the sample. In this way, array scans (i.e.

2D maps) were determined. The electric conditions of the samples were the same used to record the *z*-approach curves as described in the previous paragraph, namely, the tip was maintained at a potential of +0.50 V vs. Ag/AgCl/KCl(3M). SECM images were obtained covering an area of 100 μm x 100 μm.

Table 2 reports the open circuit potential values, $E_{ocp}$, attained by the alloys in the two test environments considered in this work.

## 3. RESULTS AND DISCUSSION

### *3.1. SECM measurements in Ringer's solution*

Imaging in scanning electrochemical microscopy is usually performed by measuring a faradaic current at an ultramicroelectrode probe (SECM tip). In our experiments, ferrocene-methanol was added to the Ringer's solution for this purpose. Separate control of the electric state of the substrate can be attained by using a bipotentiostat allowing for controlled polarization of the sample to a predefined potential. However, operation of the system under open circuit conditions is also advantageous especially to explore naturally corroding conditions. Yet natural corrosion cannot be easily guaranteed when the SECM is operated in the feedback mode because the free-diffusing redox mediator added to the electrolyte solution affects the potential of the sample. That is, the potential of the sample will be imposed by the Nernst potential of the dissolved redox mediator. Therefore, open circuit conditions, as well as both anodic and cathodic polarizations of the samples, were considered in this work.

When the protective films developed on metal surfaces exhibit electrically-insulating properties, i.e. they are effective physical barriers for electron conductivity through them, a negative feedback type of response occurs as the SECM tip approaches the specimen surface [62,63]. In this case, the faradaic current measured at the tip steadily decreases towards zero when the tip approaches the sample due to the reduced volume of electrolyte comprised between them. In order to maintain the faradaic reaction occurring at the active surface of the microelectrode tip, diffusion of the redox mediator from the bulk electrolyte must occur, but the process is progressively hindered with the reduction of the electrolyte volume adjacent to the tip. Conversely, a positive feedback type of response occurs when the SECM tip approaches the surface of the bare metal substrate [62]. The redox mediator can be recycled at the pure conductive sample surface under investigation, therefore the faradaic current measured at the tip increases for smaller tip-to-sample distances. These predictions seem to agree well with the experimental results obtained on Ti-20Mo exposed to Ringer's solution at ambient temperature, as shown in Figure 1A. In fact, smaller faradaic currents are measured above the Ti-20Mo alloy when the SECM tip is located in close proximity to the investigated surface than when the tip is placed in the bulk of the testing electrolyte, for all the applied polarizations. On the other hand, the effect of polarization can be directly related to the thickness of the oxide films formed on the

surface of the alloy at each potential value. Increasingly positive applied polarizations led to the formation of thicker oxide films, therefore less conductive towards electron mobility. Consequently, smaller faradaic currents were measured at the tip for a given tip-to-sample distance when the substrate was polarized at a more positive potential. This behaviour corresponds to a situation at which there is hindered diffusion of ferrocene-methanol towards the tip, and this species does not regenerate on the surface of the sample. That is, the general mechanism governing the faradaic current measured at the tip for ferrocene-methanol oxidation corresponds to a negative feedback effect.

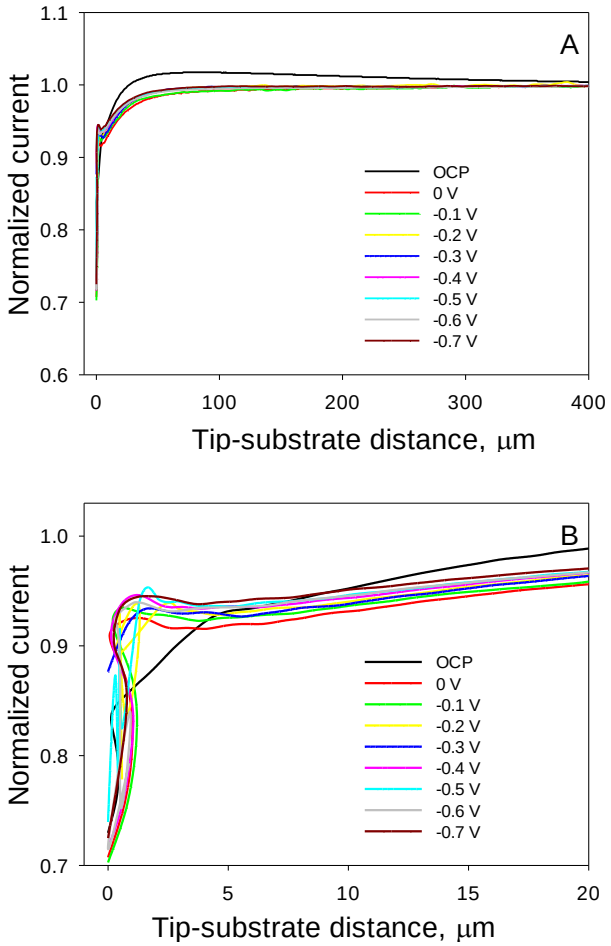


**Figure 1.** SECM normalized *z*-approach curves towards Ti-20Mo. Test environment: naturally aerated Ringer's solution. Electric conditions of the sample are given in the plot. Tip potential: +0.50 V vs. Ag/AgCl/KCl(3M) reference electrode. Scan rate: 10 μm $s^{-1}$.

Yet this description cannot fully describe the shape of the *z*-approach curves at short tip-to-sample distances as observed in Figure 1B that presents an expanded presentation of these curves for normalized distances smaller than 50. Though the values of the normalized currents are smaller than 1.0 in all cases, local features on the plots related to the development of shoulders in the curves are observed. That is, there is not a continuous and steady decrease of the faradaic current from the bulk values towards zero as the tip approaches the sample, which is the expected trend for pure negative

feedback behaviour.

It must be noticed that the apparent negative feedback behaviour is also found when unbiased Ti-20Mo is approached. But, some observations must be made in relation to the shape of the corresponding approach curve in this case. Though the open circuit potential of this alloy in Ringer's solution (namely -0.13 V vs. Ag/AgCl/KCl(3M)) is placed inside the range of polarizations considered above, the *z*-approach curve measured at the OCP does not lie between those measured for the closest anodic and cathodic polarizations (respectively at -0.10 and -0.20 V vs. Ag/AgCl/KCl(3M)). Furthermore, the *z*-approach curve for the unbiased sample shows some differences to those measured when the sample was polarized in the same environment. Two main features can be distinguished: (1) the absence of the shoulder on the curve in the small tip-to-sample distance range; and (2) the existence of a rather extended tip-to-sample distance range for which normalized currents greater than one were measured. The later implies that more redox mediator should be available at the tip/electrolyte interface at those distances than in the bulk of the electrolyte, i.e. some recycling of the redox mediator must occur at the sample surface under investigation which is sensed even at quite large distances. Hence, the discrepancy between the approach curves toward the electrode surface and the theoretical prediction must be due to a partial positive feedback effect on the electrode surface. That is, the localized concentration of ferrocene is greater than it would be on a resin surface for the same tip-to-sample distance, which only shows the blockage effect of the redox mediator transferring from bulk solution to tip surface. The tip current decreases less and a partial positive feedback occurs.

It is considered that metallic biomaterials should be sufficiently chemically-inert when placed in the human body for them to be employed as implants. Though there is no chemically-inert material, some metals are regarded acceptable for implant application when they remain in their stable passive regime throughout the whole range of water stability. Yet, passive films formed by oxides of the metal are not perfect insulating physical barriers, but rather exhibit semiconductor behaviour. That is, electron transfer reactions may occur at their surface though often big overpotentials might be required for the electrons to be driven through these surface films. On the other hand, it has also been demonstrated that passive films exhibit instabilities related to localized film breakdown and subsequent passive film repair, at potentials well below their corresponding breakdown potentials, that is, at the typical electrical and chemical conditions met in the human body [64,65]. In this way, even for very unreactive metals such as titanium and its alloys, release of metal ions into adjacent tissues can occur [65]. So far, it has not been possible to ascertain whether instabilities in passive films occur exclusively at defects in the oxide films or they are an intrinsic characteristic of passive layers. In fact, oxide films formed on alloys usually present defects related to inclusions, grain boundaries, or heterogeneous distributions of the alloying elements, which occur at the surface of the buried metal substrate. Yet passive layer instabilities have also been observed in high purity valve metals such as titanium and tantalum [66,67].

Analogously, *z*-approach curves were also measured for the tantalum alloys immersed in Ringer's solution, and they are displayed in Figure 2. For Ti-30Ta, all the plots initially exhibit an

increase in the faradaic current measured at the tip with respect to the limiting diffusion value measured in the bulk of the solution (cf. Figure 2A). This behaviour occurs for distances smaller than 300 μm regardless the electric condition operating at the substrate, namely for both the unbiased and the polarized substrate. This slow increase is followed by a fast decrease when the hindered diffusion of ferrocene-methanol towards the tip becomes the main contribution to the overall current, namely for distances smaller than 3 μm. It must also be noticed that the *z*-approach curves of the polarized substrate can be superimposed on that measured at the OCP until the maximum current is attained for distances ca. 5 μm. That is, the partial positive feedback effect experienced by this alloy is independent of the thickness of the passive film developed on the surface of the material. Conversely, the electrical condition of the substrate has a major effect when the tip is located in close proximity to the substrate (i.e, for distances smaller than 3 μm). Thus, the extent of the negative feedback effect, which is a direct measure of the insulating characteristics of the approached surface, varies with the applied potential in the same manner that for the Ti-20Mo alloy (cf. Figure 1A).

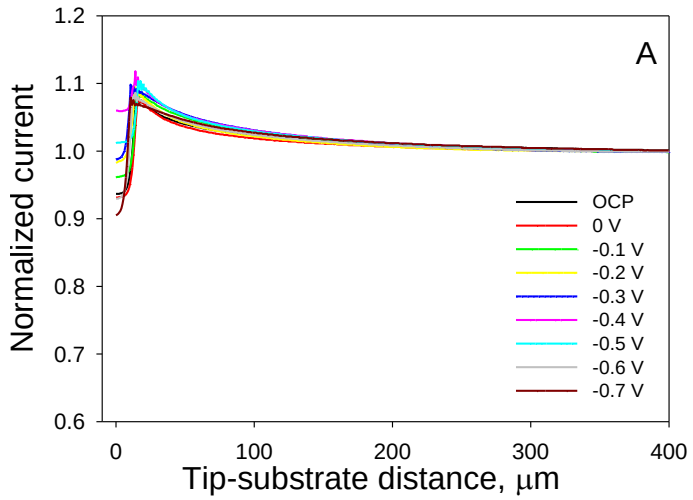


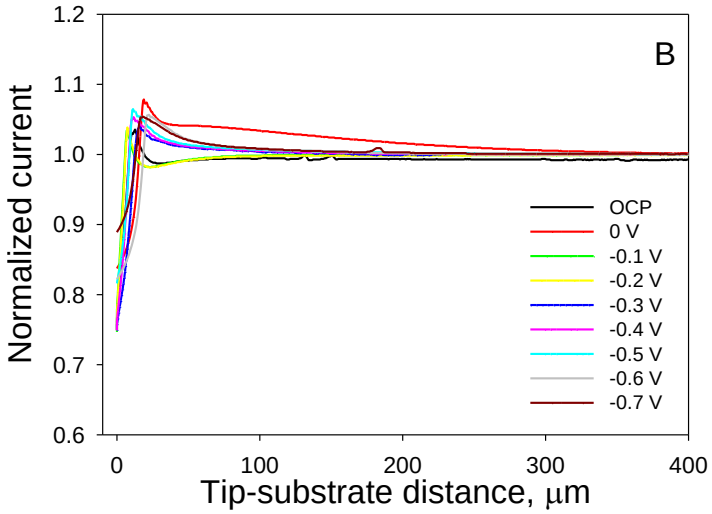

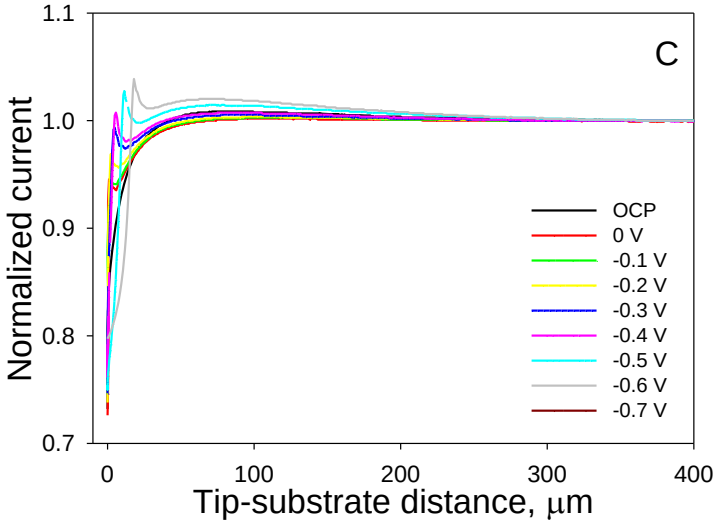


**Figure 2.** SECM normalized *z*-approach curves towards different Ti-Ta alloys: (A) Ti-30Ta, (B) Ti-40Ta, and (C) Ti-50Ta. Test environment: naturally aerated Ringer's solution. Electric conditions of the samples are given in the plot. Tip potential: +0.50 V vs. Ag/AgCl/KCl(3M) reference electrode. Scan rate: 10 μm $s^{-1}$.

In the case of the *z*-approach curves measured for Ti-40Ta and Ti-50Ta, a new situation is found. Depending on the value of the potential applied to the sample, the shape of the approach curve will correspond to that described for Ti-20Mo or to the corresponding to Ti-30Ta. That is, for the less negative potentials considered, the normalized current slowly decreases when the tip is moved towards smaller *z* values until a maximum is defined close to the surface. Conversely, at the more negative potentials, the normalized current steadily grows to produce values greater than 1.0 while the tip-to-sample distance is reduced, until a maximum is defined for distances ca. 20 μm, and then the current decreases very quickly in the close proximity to the electrode. A transition between the two behaviours is observed at an intermediate polarization applied to the samples, which is characteristic for each material (namely, between -0.20 and -0.30 V vs. Ag/AgCl/KCl(3M) for Ti-40Ta, and between -0.40 and -0.50 V vs. Ag/AgCl/KCl(3M) for Ti-50Ta).

### *3.2. SECM measurements in 0.1 M NaCl solution*

In order to further investigate the differences in surface chemical activity amongst the titanium alloys under consideration, a similar set of experiments was conducted for the materials immersed in 0.1 M NaCl solution. The electrolyte solution was chosen as to simplify the number of chemical species present in the simulated physiological environment, thus avoiding possible combined effects of the different components at this stage. Sodium chloride was then chosen as to contain the main reacting species in the environments is the chloride ion, which is the main aggressive species for passive film breakdown [64] without significantly changing the pH of the environment and with only

one counter-ion present. In this way, variations in surface activity among the materials should be more easily interpreted.

Figure 3 depicts the *z*-approach curves determined for the four titanium alloys, which were tested at different electrical conditions in the 0.1 M NaCl solution. For the Ti-20Mo alloy, smaller faradaic currents are measured when the tip located in close proximity to the investigated surface than when the tip is placed in the bulk of the testing electrolyte, for all the applied polarizations (cf. Figure 3A). Yet two different situations can be distinguished in the approach curves as the tip is progressively moved towards the surface from the bulk of the electrolyte (i.e., the tip is moved respective to the *Z* axis). Firstly, for substrate potentials positive to -0.30 V vs. Ag/AgCl/KCl(3M) (i.e., for $0 \geq E \geq -0.20$ V vs. Ag/AgCl/KCl(3M)), the current is observed to decrease steadily. Conversely, for applied potentials in the range $-0.40 \geq E \geq -0.70$ V vs. Ag/AgCl/KCl(3M), the faradaic current measured at the tip initially increases with respect to the limiting diffusion value, and this is followed by a fast decrease when the hindered diffusion of ferrocene-methanol towards the tip becomes the main contribution to the overall current.

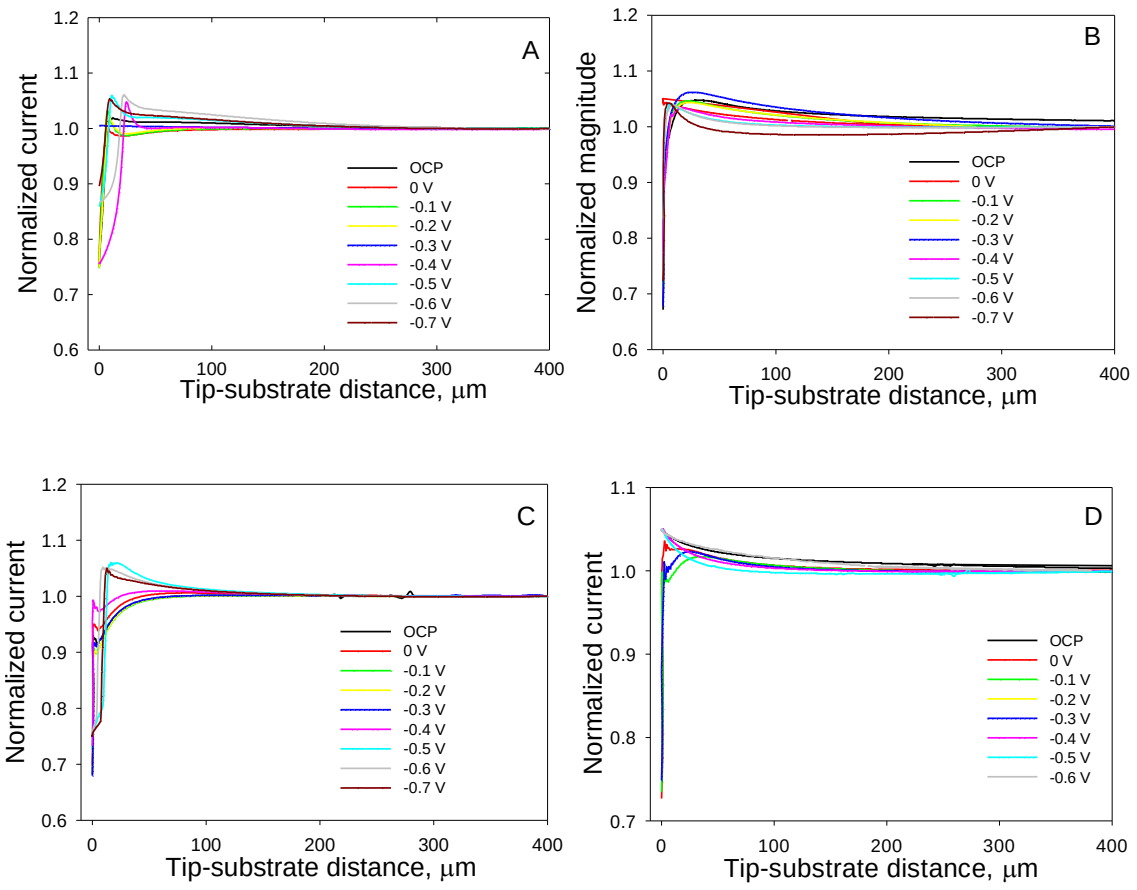


**Figure 3.** SECM normalized *z*-approach curves towards different Ti-Mo and Ti-Ta alloys: (A) Ti-20Mo, (B) Ti-30Ta, (C) Ti-40Ta, and (D) Ti-50Ta. Test environment: naturally aerated 0.1 M NaCl solution. Electric conditions of the samples are given in the plot. Tip potential: +0.50 V vs. Ag/AgCl/KCl(3M) reference electrode. Scan rate: 10 μm $s^{-1}$.

From the point of view of the shape of the approach curves, a transition situation occurs around -0.30 V vs. Ag/AgCl/KCl(3M), for which the tip current is almost independent of the tip-substrate distance. In other words, no measurable feedback effect occurs at this polarization. This kind of behaviour has been reported recently for titanium grade 7 alloys, where the whole area exposed to the aqueous environment activated at potentials below -0.45 V vs. Ag/AgCl/KCl(3M) [51].

It must be noticed that the negative feedback behaviour is also found when unbiased Ti-20Mo is approached. But, a significant observation must be made in relation to the shape of the corresponding approach curve in this case. Though the open circuit potential of this alloy in 0.1 M NaCl (namely -0.04 V vs. Ag/AgCl/KCl(3M), effectively more positive than the transition potential reported above, the current transient also exhibits an initial increase in the tip current as the surface is approached, and normalized current values smaller than 1.0 are only observed in very close proximity to the surface. That is, the behaviour of the alloy under spontaneously-developed electric conditions can be significantly different from those generated during conventional electrochemical experiments, which are based on the application of either a current or a potential perturbation to the system that is applied to the overall material surface exposed to the test environment. Conversely, under spontaneously attained electric conditions, i.e. under open circuit conditions, microcells are formed on the exposed surface. Therefore, a spatial distribution of microanodes and microcathodes is developed for the electrochemical processes occurring at the surface to be maintained, and local potential differences take place. This observation is a strong support for the need of spatially resolved microelectrochemical techniques such as SECM to be employed in order to adequately monitor the physicochemical behaviour of alloys in aqueous environments. And even in this case, experiments must also be performed on unbiased samples. From the foregoing it should not be considered that experiments under polarization conditions are useless, for the response of the system to given transient conditions can be thus investigated, but rather to regard unbiased conditions as the main objective in the work. A similar observation can be made in relation to the use of conventional electrochemical techniques, such as potentiodynamic polarization curves and electrochemical impedance spectroscopy (EIS). Though these techniques average the behaviour of the whole surface, relevant information on the system regarding general trends on passivation, stability of the passive state, localized corrosion and even metal dissolution are still gathered. And they provide a rather quick and straightforward experimental procedure for the general trends of different materials in aqueous environments to be distinguished at least in a first stage.

Titanium alloys containing tantalum were also investigated using the same experimental procedures during their exposure to 0.1 M NaCl. Figure 3 depicts the *z*-approach curves for the three materials. In all cases, a negative feedback behaviour is found too. In the case of Ti-30Ta alloy (see Figure 3B), when the potential applied to the surface is increased we observe an increase in normalized current intensity near the surface, that is followed by a sharp decrease as a result of hindered diffusion of ferrocene-methanol to the tip. This behaviour, which only occurred for the more negative polarizations in the case of the Ti-20Mo alloy, arises from the establishment of a competition between

hindered diffusion of the redox mediator to the tip (negative feedback) and its regeneration through a chemical reaction of the oxidized species with the substrate, the later occurring slower than the rate of diffusion.

For the Ti-40Ta and Ti-50Ta alloys, the two trends reported for the *z*-approach curves of the Ti-20Mo alloy are observed again (cf. Figures 3C and 3D).

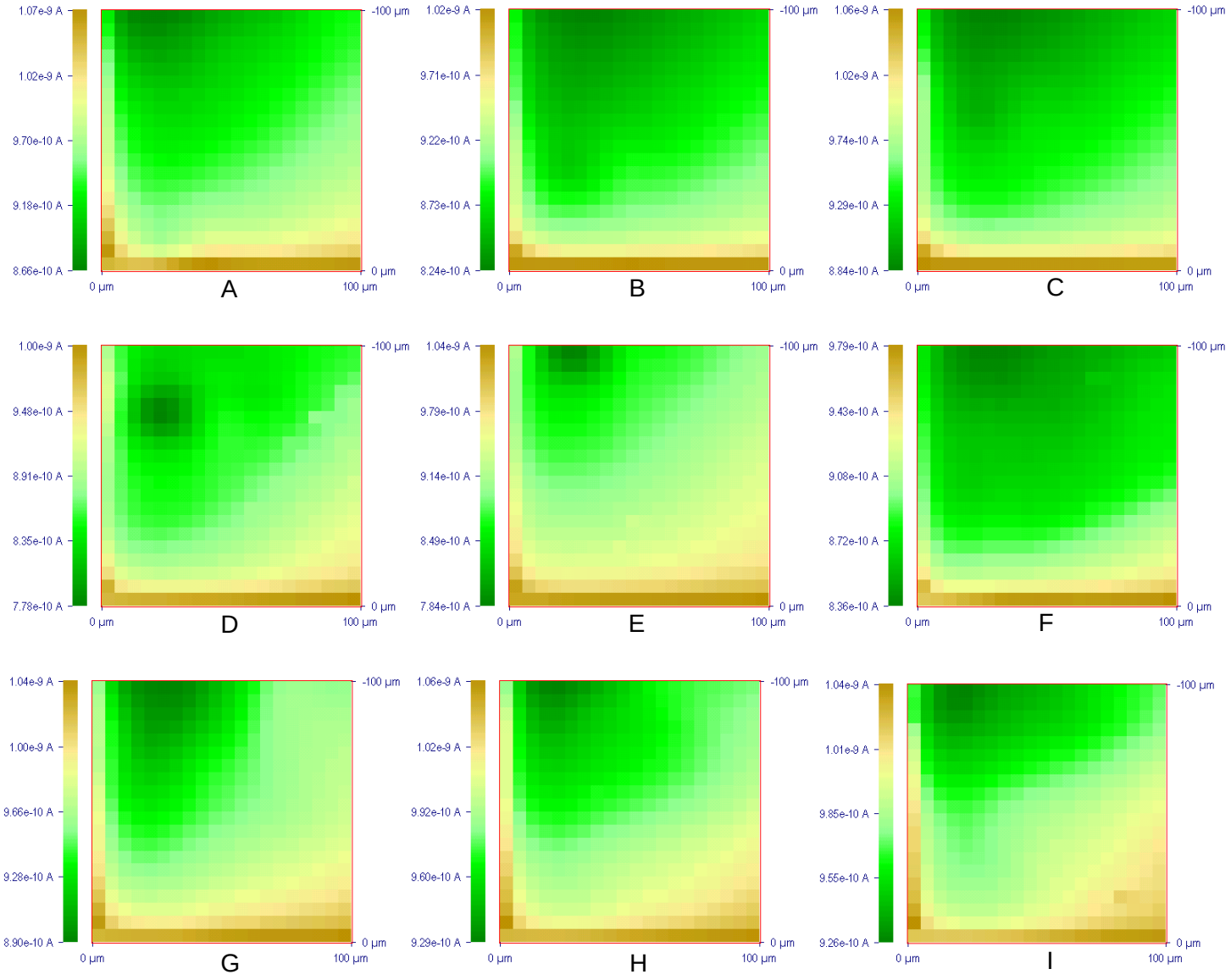


**Figure 4.** Images generated by SECM of a Ti-20Mo alloy immersed in 0.1 M NaCl air-saturated aqueous solution. Electric condition of the sample: (A) unbiased, and (B-I) under polarization. Applied potentials: (B) 0, (C) -0.10, (D) -0.20, (E) -0.30, (F) -0.40, (G) -0.50, (H) -0.60, and (I) -0.70 V vs. Ag/AgCl/KCl(3M) reference electrode. Tip–substrate distance: 10 µm. Tip potential: +0.50 V vs. Ag/AgCl/KCl(3M) reference electrode. Scan rate: 30 µm $s^{-1}$. The figures represent an area of 100 µm × 100 µm in *x* and *y* directions.

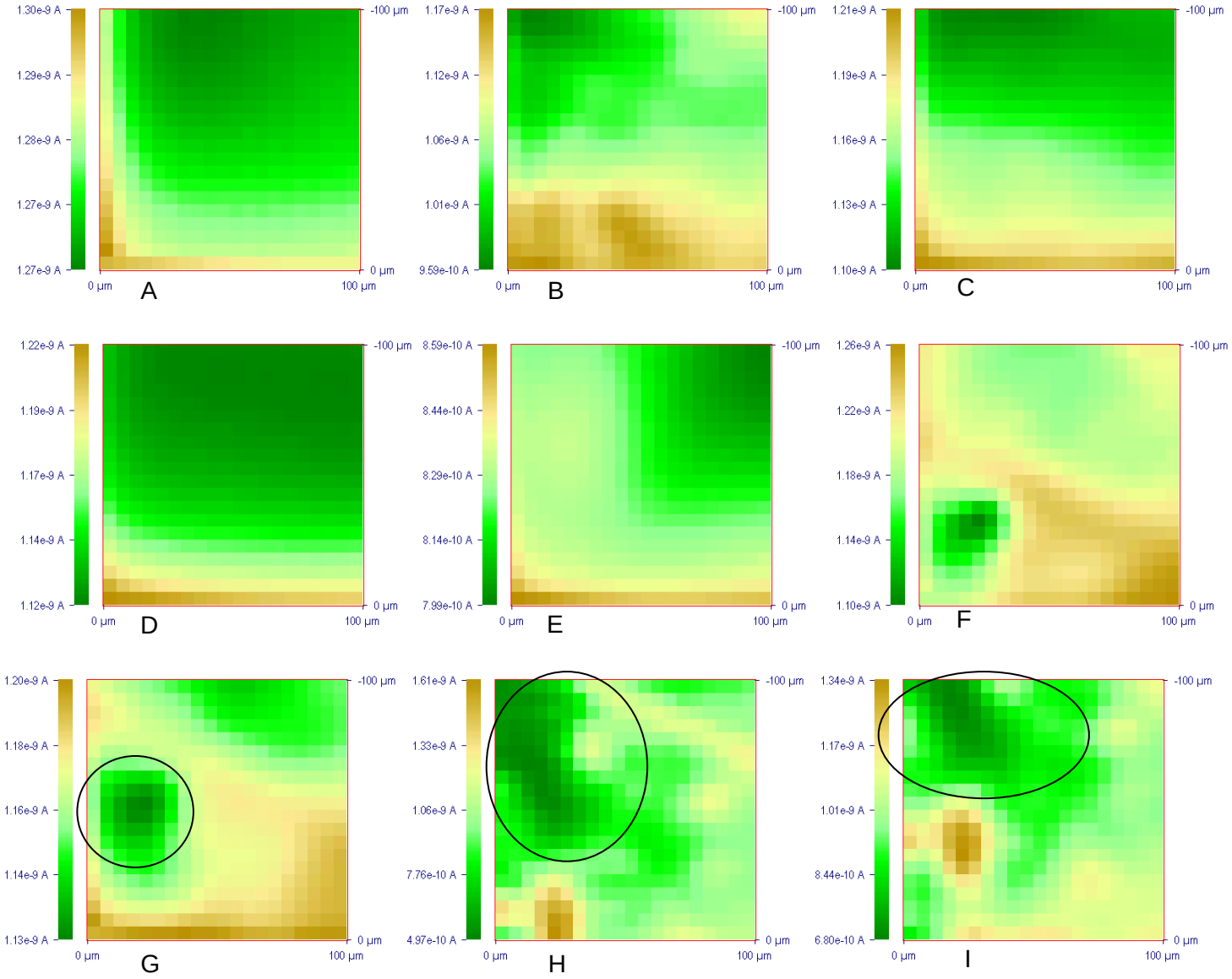


**Figure 5.** Images generated by SECM of a Ti-30Mo alloy immersed in 0.1 M NaCl air-saturated aqueous solution. Electric condition of the sample: (A) unbiased, and (B-I) under polarization. Applied potentials: (B) 0, (C) -0.10, (D) -0.20, (E) -0.30, (F) -0.40, (G) -0.50, (H) -0.60, and (I) -0.70 V vs. Ag/AgCl/KCl(3M) reference electrode. Tip–substrate distance: 10 µm. Tip potential: +0.50 V vs. Ag/AgCl/KCl(3M) reference electrode. Scan rate: 30 µm $s^{-1}$. The figures represent an area of 100 µm × 100 µm in *x* and *y* directions.

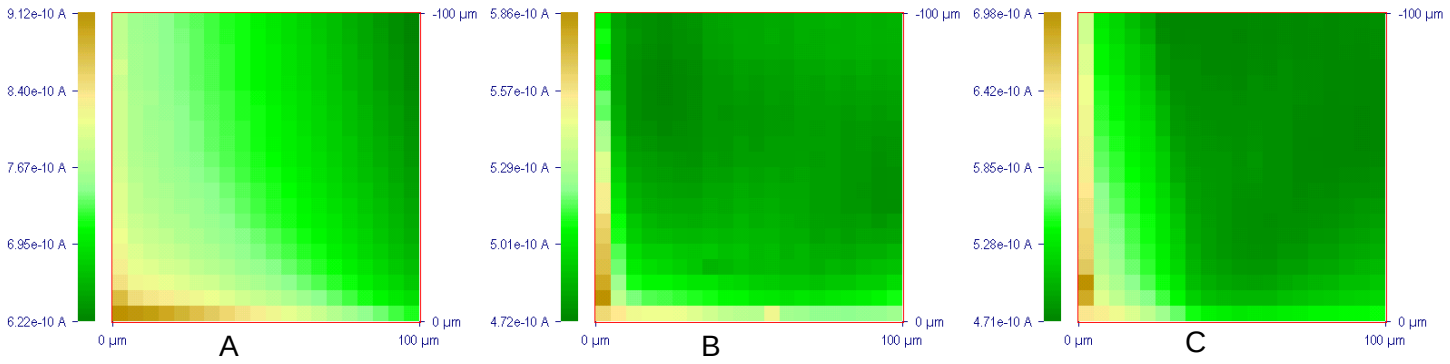

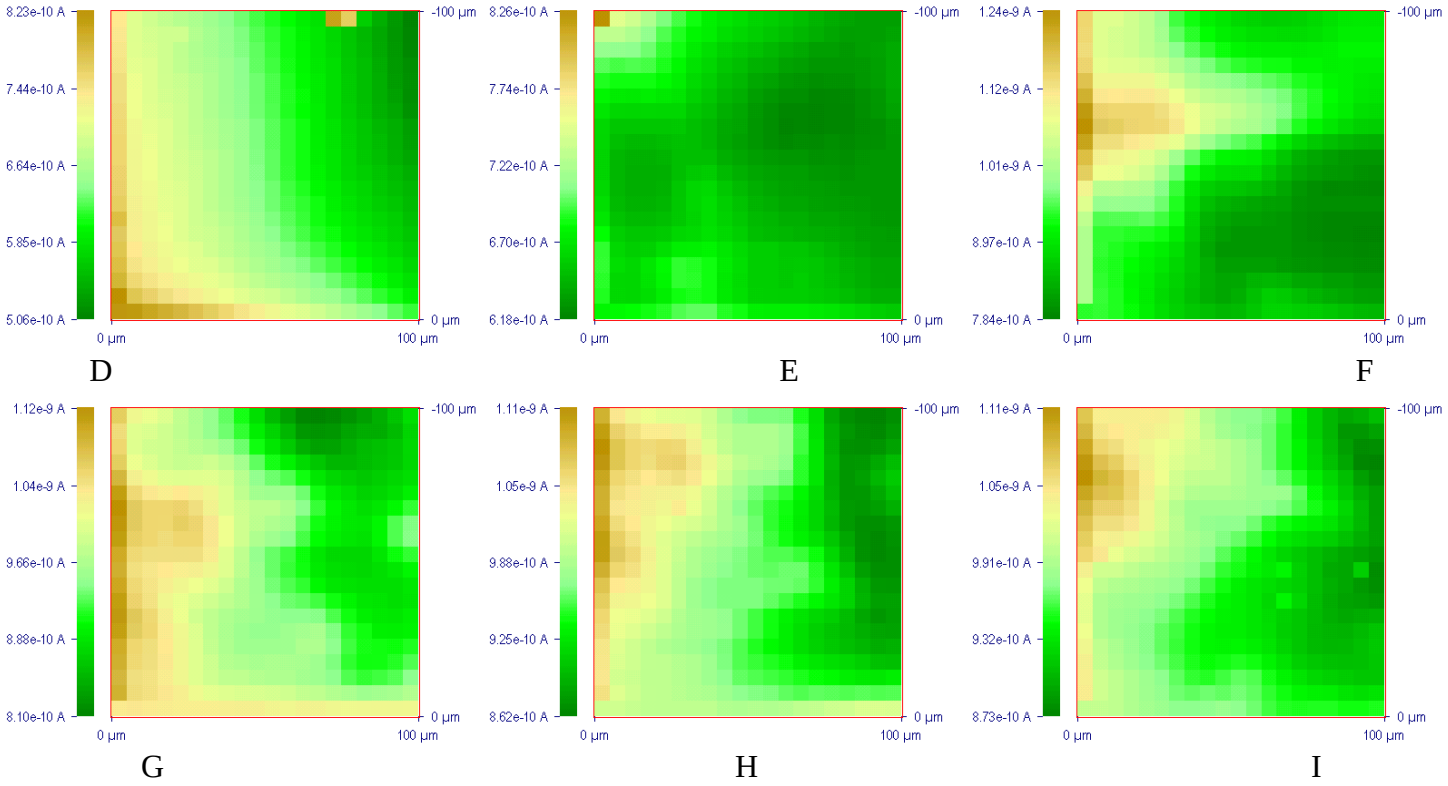


**Figure 6.** Images generated by SECM of a Ti-40Mo alloy immersed in 0.1 M NaCl air-saturated aqueous solution. Electric condition of the sample: (A) unbiased, and (B-I) under polarization. Applied potentials: (B) 0, (C) -0.10, (D) -0.20, (E) -0.30, (F) -0.40, (G) -0.50, (H) -0.60, and (I) -0.70 V vs. Ag/AgCl/KCl(3M) reference electrode. Tip–substrate distance: 10 µm. Tip potential: +0.50 V vs. Ag/AgCl/KCl(3M) reference electrode. Scan rate: 30 µm $s^{-1}$. The figures represent an area of 100 µm × 100 µm in *x* and *y* directions.

Although normalized currents smaller than 1.0 are found at all tip-substrate distances when the samples were subjected to small negative polarizations (i.e. apparent negative feedback behaviour), a range of current values in excess of 1 was observed in the *z*-approach curves measured for the sample with an applied potential equal or more negative than -0.50 V vs. Ag/AgCl/KCl(3M).

There was an increase in the normalized current near the surface and then a sharp decrease as soon as we get closer to the surface, thus showing in all three cases a negative feedback. As the polarization increases, the obtained line scans do not produce significant variation in the reactivity of the surface. In the case of the unbiased samples, the shape of the curve corresponds to the type exhibited in the case of the less negative polarizations for Ti-40Ta (see Figure 3C), whereas the opposite occurs for Ti50 Ta (Figure 3D).

Variations in the electrochemical behaviour of a given material when exposed to different environments can be readily observed by comparing the *z*-approach curves measured for each titanium alloy when exposed to Ringer's and to 0.1 M NaCl solutions. In general, there is greater surface activity in the alloys during immersion in 0.1 M NaCl solution for the less negative polarizations,

observed as bigger differences between the minimum and the maximum normalized current values in the corresponding curves.

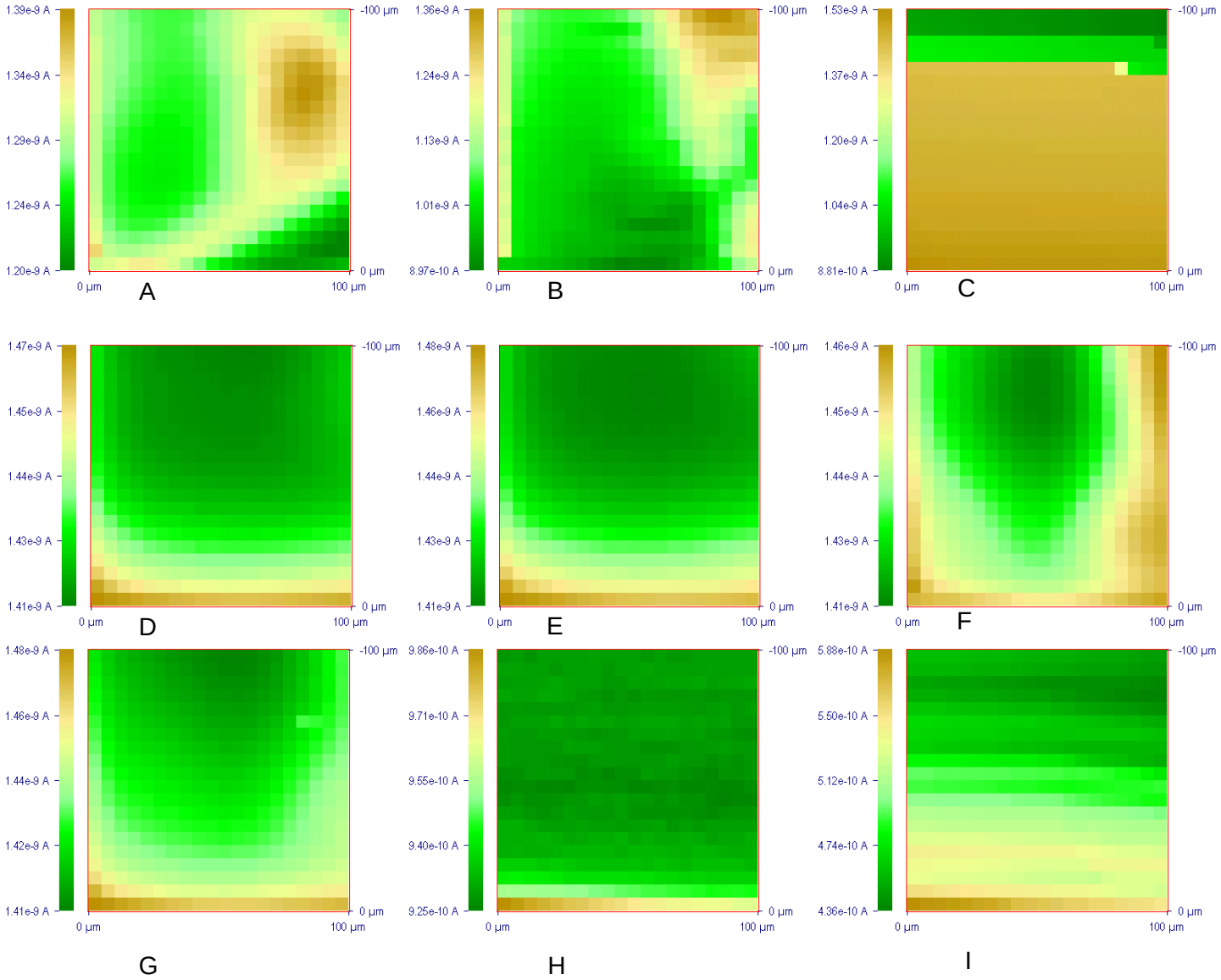


**Figure 7.** Images generated by SECM of a Ti-50Mo alloy after immersion in 0.1 M NaCl air-saturated aqueous solution. Electric condition of the sample: (A) unbiased, and (B-I) under polarization. Applied potentials: (B) 0, (C) -0.10, (D) -0.20, (E) -0.30, (F) -0.40, (G) -0.50, (H) -0.60, and (I) -0.70 V vs. Ag/AgCl/KCl(3M) reference electrode. Tip–substrate distance: 10 µm. Tip potential: +0.50 V vs. Ag/AgCl/KCl(3M) reference electrode. Scan rate: 30 µm $s^{-1}$. The figures represent an area of 100 µm × 100 µm in *x* and *y* directions.

In order to detect changes in surface structure of various tested titanium alloys, SECM images were registered over an arbitrary portion of the exposed surface for the four alloys during immersion in 0.1 M NaCl. The tip was maintained at a potential of +0.50 V vs. Ag/AgCl/KCl(3M). The experimental procedure was as it follows. Once located the surface from the measurement of the *z*-

approach curve for a given electric condition of the sample, as described above, the tip was retracted 10 μm from the surface, and scan arrays covering an area of 100 x 100 $\mu m^2$ were registered by moving the microelectrode tip in an *xy* plane parallel to the sample. The obtained SECM images are shown in Figures 4-7.

The images in Figure 4 show a marked difference in the extent of chemical activity between the bottom and top of the maps recorded for the Ti-20Mo alloy. A positive feedback type of behaviour occurs in the lower part of the scanned map, which extends over an increasing area as the polarization of the sample is made more negative. Though the area of higher faradaic currents grows in size, the absolute values of the current remain almost constant throughout the measurement time. On the contrary, the smallest values of the current in the maps, increases from a minimum value of 0.824 nA in the image measured when the sample was polarized at 0 V vs. Ag/AgCl/KCl(3M), to current values greater than 0.926 nA for the map corresponding to $E$ = -0.70 V vs. Ag/AgCl/KCl(3M).

In the case of the Ti30Ta alloy (see Figure 5), there is a significant change in surface activity for polarizations $E \leq$ -0.40 V vs. Ag/AgCl/KCl(3M). A big portion of the imaged surface becomes activated, giving rise to a sharp increase in the values of the faradaic currents measured at the tip when passing above that region (cf. Figure 5F). Simultaneously, there is also a depletion of the currents measured over the area portions indicated with an ellipse. It is also interesting to note that the regions of lower currents are shifting from one place to another over the scanned surface, and cover a greater portion of the surface as the applied potential is set more negative. In this way, the smaller currents measured in those regions change from initial values close to 1.13 nA to values as small as 0.680 nA in the image for $E$ = -0.70 V vs. Ag/AgCl/KCl(3M). The regions on the surface with increased currents correspond to an enhanced recycling of the redox mediator which is expected to occur in zones with thin oxide layer. But regeneration of ferrocene-methanol from ferrocinium ion at those sites effectively requires an oxidation reaction to occur there, with the result of oxide layer thickening. Thus, the zones with lower currents occur at other locations on the surface in the subsequent SECM images, and the described process occurs again.

From the inspection of the SECM images for Ti-40Ta given in Figure 6, it can be deduced that there is a clear increase in the magnitude of the cathodic currents for $E \leq$ -0.40 V vs. Ag/AgCl/KCl(3M). The surface becomes progressively activated in the direction from left to right for all the applied polarizations. There is a change of trend for Ti-30Ta and Ti-40Ta alloys, which coincides with the documented existence of a major transition in the electrochemical characteristics of Ti-Ta alloys occurring in the interval from Ti-20Ta to Ti-40Ta alloys, the first having a behaviour more similar to that of pure Ti, while the later having a behaviour closer to that of pure Ta [38].

Finally, the SECM images for Ti-50Ta alloys given in Figure 7 showed the highest maximum values for the faradaic current, even in the case of the map measured while the sample was left at its corresponding OCP. Next, the electrochemical activity of the surface changes with the applied polarizations. Thus, for both OCP and $E$ = 0 V vs. Ag/AgCl/KCl(3M), currents in the range of 1.36-1.39 nA were observed, related to the development of an active area at the top of the image (see

Figures 7A and 7B, respectively). For polarizations of -0.10 and -0.20 V vs. Ag/AgCl/KCl(3M), a more homogeneous distribution of the current over the entire area is found. And significantly smaller currents (namely in the order of 0.98 nA), were measured for $E \leq$ -0.30 V vs. Ag/AgCl/KCl(3M). In a previous investigation it was shown on the basis of XRD analysis that the alloys Ti-20Ta, Ti-40Ta, Ti-60Ta, and Ti-80Ta are multiphase microstructures, and the ratios of α and β phases vary among the materials [17,68]. This might explain the reported differences in surface chemical activity of these alloys reported in this work. α and β phases were present in theTi-20Ta and Ti-40Ta alloys microstructure, while for Ti-60Ta and Ti-80Ta alloys only the β phase was present. As the amount of Ta increases so will the volume fraction of the β phase, observing the lamellar and needle morphology of the α phase in three of the studied alloys (Ti-30Ta, Ti-40Ta, Ti-50Ta).

A major common feature observed in the microelectrochemical behaviour between the Ti-20Mo alloy and the Ta-containing alloys can be derived form our SECM results concerning the activation of surface chemical activity in the materials. It was reported that a transition potential could be established at $E$ = -0.30 V vs. Ag/AgCl/KCl(3M) for Ti-20Mo exposed to 0.1 M NaCl solution as derived from *z*-approach curves. At this potential there is a change in the shape of the curves corresponding to the relative contributions of partial positive feedback and of hindered diffusion (i.e. negative feedback behaviour) which depend on the tip-to-sample distance. And this transition potential could be related to the observation of greater variation in surface activity for the alloy from the corresponding SECM images. Analogously, a correlation between the change in the shape of the *z*-approach curves and an increase in the surface activity registered in the SECM has also been established for the tested Ti-Ta alloys, and this transition occurred for polarizations between -0.30 and -0.40 V vs. Ag/AgCl/KCl(3M) in all the cases. That is, the activation of surface activity coincides with an increase in the values of the tip current measured at the distance of closest approach in the *z*-approach curves, when the negative feedback effect is no longer the main factor affecting the current flowing at the tip. Recycling of the redox mediator occurs on the activated surface below the tip leading to a deviation of the expected behaviour for negative feedback on an insulator. However, when the tip is located in very close proximity to the surface, geometric factors determine the tip current. This effect results from the blockage to diffusion imposed by the substrate that hinders ferrocene-methanol to diffuse towards the active surface of the microelectrode in a greater extent than it can be regenerated from ferrocinium ion according to its regeneration rate.

## 4. CONCLUSIONS

SECM is an electrochemical tool that allows for characterizing the surface electrochemical activity occurring on titanium-based alloys with spatial resolution. Potentiostatically-controlled variation of the substrate potential causes localized changes in the physicochemical characteristics of the oxide layers formed on different Ti-Mo and Ti-Ta alloys, which eventually lead to the local activation of reaction sites on the surface of the materials.

SECM analysis distinguishes differences in the chemical activity of the alloys which are related to their composition, as well as changes for a given material during exposure to different environments. The titanium alloys investigated in this work exhibit greater chemical activity when immersed in 0.1 M NaCl compared to their performance in Ringer's solution.

Though the *z*-approach curves could be generally related to a negative feedback type of behaviour for the electrochemical conversion of the redox mediator at the ultramicroelectrode tip regardless the electric condition of the samples, the experimental data are always greater than it could be expected for the tip approaching a truly insulating substrate. Partial positive feedback effects are detected, which compete with geometric constraints as to determine the shape of the *z*-approach curves for different polarizations of the samples. A transition potential range is determined from the changing shapes of the *z*-approach curves, which has been readily related to the activation of sites on the surface of the materials for the regeneration of the electrochemical mediator.

For the titanium alloys immersed in 0.1 M NaCl solution, surface chemical activation occurs at polarizations between -0.30 and -0.40 V vs. Ag/AgCl/KCl(3M) for the investigated Ti-Ta alloys. This change is more noticeable for the alloys with greater contents in tantalum, which can be related to the predominance of the β phase at the surface of the material.

ACKNOWLEDGMENTS

This work was supported by the Ministerio de Ciencia e Innovación (Madrid, Spain) and the European Regional Development Fund (Brussels, Belgium) under Grant Number CTQ2009-14322/PPQ. A Research Training Grant awarded to J.I. by the MICINN (*Programa de Formación de Personal Investigador*) is gratefully acknowledged. G.C., D.M. and D.S. acknowledge the Romanian CNCS Program for the project PN-II-ID-PCE-2011-3-0218, no. 266. Thanks are due to Dr. T. Gloriant at INSA Rennes (France) for kindly providing the titanium alloys used in this work.

## References

1. M. Geetha, A.K. Singh, R. Asokamani and A.K. Gogia, *Prog. Mater. Sci.* 54 (2009) 397.
2. *ASM Handbook. Corrosion*, Vol. 13, 9th edn. ASM International, Metals Park, OH (1987), p. 669.
3. M. Pourbaix, *Atlas of electrochemical equilibria in aqueous solutions*. NACE, Houston (1974), p. 213.
4. M. Niinomi, *J. Mech. Behav. Biomed. Mater.* 1 (2008) 30.
5. M. Long and H.J. Rack, *Biomaterials* 19 (1998) 1621.
6. S.G. Steinemann, in: *Evaluation of Biomaterials*, (G.D. Winter, J.L. Leray and K. de Groot, Eds.). Wiley, New York (1980), p. 1.
7. M. Niinomi, D. Kuroda, M. Morinaga, Y. Kato and T. Yashiro, in: *Non-aerospace applications of titanium*, (F.H. Froes, P.G. Allen, M. Niinomi, Eds.). The Minerals, Metals and Materials Society, Warrendale (1998), p. 217.
8. D. Bombac, M. Brojan, P. Fajfar, F. Kosel and R. Turk, *RMZ – Mater. Geoenviron.* 54 (2007) 471.
9. R. Godley, D. Starosvetsky and I. Gotman, *J. Mater. Sci.-Mater. Med.* 17 (2006) 63.
10. Q. Yao, J. Sun, H. Xing and W. Guo, *Trans. Nonferrous Met. Soc. China* 17 (2007) 1417.
11. Y.L. Zhou, M. Niinomi and T. Akahori, *Mater. Sci. Eng. A* 371 (2004) 283.
12. Y.L. Zhou, M. Niinomi, T. Akahori, H. Fukui and H. Toda, *Mater. Sci. Eng. A* 398 (2005) 28.

13. E.A. Trillo, C. Ortiz, P. Dickerson, R. Villa, S.W. Stafford and L.E. Murr, *J. Mater. Sci.-Mater. Med.* 12 (2001) 283.
14. Y.L. Zhou, M. Niinomi, T. Akahori and H. Fukui, *Mater. Sci. Forum* 479 (2005) 2309.
15. Y.L. Zhou and M. Niinomi, *J. Alloy Compd.* 466 (2008) 535.
16. Y.L. Zhou, M. Niinomi and T. Akahori, *Mater. Sci. Eng. A* 483-484 (2008) 153.
17. D. Mareci, R. Chelariu, D.M. Gordin, G. Ungureanu and T. Gloriant, *Acta Biomater.* 5 (2009) 3625.
18. Y.L. Zhou and M. Niinomi, *Mater. Sci. Eng. C* 29 (2009) 1061.
19. D. Mareci, R. Chelariu, G. Ciurescu, D. Sutiman and T. Gloriant, *Mater. Corros.* 61 (2010) 768.
20. V.R. Jablokov, M.J.Nutt. M.E. Richelsoph and H.L. Freese, *J. ASTM Int.* 2 (2005) 491.
21. S. Kumar and T.S.N. Sankara Narayanan, *J. Dent.* 36 (2008) 500.
22. N.T.C. Oliveira and A.C. Guastaldi, *Corros. Sci.* 50 (2008) 938.
23. N.T.C. Oliveira and A.C. Guastaldi, *Acta Biomater.* 5 (2009) 399.
24. D. Mareci, R. Chelariu, D.M. Gordin, M. Romas, D. Sutiman and T. Gloriant, *Mater. Corros.* 61 (2010) 829.
25. Z. Cai, M. Koike, H. Sato, M. Brezner, Q. Guo, M. Komatsu, O. Okuno and T. Okabe, *Acta Biomater.* 1 (2005) 353.
26. W.F. Ho, W.K. Chen, S.C. Wu and H.C. Hsu, *J. Mater. Sci.-Mater. Med.* 19 (2008) 3179.
27. M. Niinomi, *Mater. Sci. Eng. A* 243 (1998) 231.
28. X. Tang, T. Ahmed and H.J. Rack, *J. Mater. Sci.* 35 (2000) 1805.
29. R. Banerjee, S. Nag, J. Stechschulte and H.L. Fraser, *Biomaterials* 25 (2004) 3413.
30. M. Geetha, A.K. Singh, K. Muraleedharan, A.K. Gogia and R. Asokamani, *Alloys Compd.* 384 (2004) 131.
31. N. Sakaguchi, M. Niinomi, T. Akahori, J. Takeda and H. Toda, *Mater. Sci. Eng. C* 25 (2005) 363.
32. S. Nag, R. Banerjee and H.L. Fraser, *Mater. Sci. Eng. C* 25 (2005) 357.
33. I. Cvijović-Alagić, Z. Cvijović, S. Mitrović, V. Panić and M. Rakin, *Corros. Sci.* 53 (2011) 796.
34. M.S. Verani , G.W. Guidry, J.J. Mahamarian, S. Nishmura, T. Athanasoulis, R. Roberts and J.L. Lacy, *J. Am. Coll. Cardiol.* 20 (1992) 1490.
35. H. Prigent, P. Pellen-Mussi, G. Cathelineau and M. Bonnaure-Lallet, *J. Biomed. Mater. Res.* 32 (1998) 200.
36. *ASM Handbook. Corrosion*, Vol. 13, 9th edn. ASM International, Metals Park, OH (1987), p. 725.
37. K.A. de Souza and A. Robin, *Mater. Corros.* 55 (2004) 853.
38. C.R. Bishop and R.L. Powell, *Corrosion* 18 (1962) 205.
39. K.A. de Souza and A. Robin, *Mater. Chem. Phys.* 103 (2007) 351.
40. A.J. Bard, F.-R.F. Fan, J. Kwak and O. Lev, *Anal. Chem.* 61 (1989) 132.
41. S.E. Pust, W. Maier and G. Wittstock, *Z. Phys. Chem*. 222 (2008) 1463.
42. L. Niu, Y. Yin, W. Guo, M. Lu, R. Qin and S. Chen, *J. Mater. Sci.* 44 (2009) 4511.
43. R.M. Souto, S. Lamaka and S. González, in: *Microscopy: Science, technology, applications and education*, Vol. 3, (A. Méndez-Vilas and J. Díaz, Eds.). Formatex Research Center, Badajoz (2010), p. 2162.
44. N. Casillas, S.J. Charlebois, W.H. Smyrl and H.S. White, *J. Electrochem. Soc.* 140 (1993) L142.
45. N. Casillas, S.J. Charlebois, W.H. Smyrl and H.S. White, *J. Electrochem. Soc.* 141 (1994) 636.
46. L.F. Garfias-Mesias, M. Alodan, P.I. James and W.H. Smyrl, *J. Electrochem. Soc.* 145 (1998) 2005.
47. S.E. Pust, D.Scharnweber, C.N. Kirchner and G. Wittstock, *Adv. Mater.* 10 (2007) 878.
48. S.E. Pust, D.Scharnweber, S. Baunack and G. Wittstock, *J. Electrochem. Soc.* 154 (2007) C508.
49. S.B. Basame and H.S. White, *Anal. Chem.* 71 (1999) 3166.
50. S.B. Basame and H.S. White, *Proc. Electrochem. Soc.* 99-5 (1999) 15.
51. R. Zhu, Z. Qin, J.J. Noël, D.W. Shoesmith and Z. Ding, *Anal. Chem.* 80 (2008) 1437.
52. H. Morisaki, H. Ono and K. Yazawa, *J. Electrochem. Soc.* 135 (1988) 381.

53. H. Morisaki, H. Ono and K. Yazawa, *J. Electrochem. Soc.* 136 (1989) 1710.
54. S.B. Basame and H.S. White, *J. Phys. Chem.* 99 (1995) 16430.
55. S.B. Basame and H.S. White, *J. Phys. Chem.* 102 (1998) 9812.
56. S.B. Basame and H.S. White, *Langmuir* 15 (1999) 819-825.
57. R.M. Souto, Y. González-García and S. González, *Corros. Sci.* 47 (2005) 3312.
58. R.M. Souto, Y. González-García and S. González, *Prog. Org. Coat.* 65 (2009) 435.
59. R. Zhu, C. Nowierski, Z. Ding, J.J. Noël and D.W. Shoesmith, *Chem. Mater.* 19 (2007) 2533.
60. R.M. Wightman and D.O. Wipf, in: *Electroanalytical Chemistry*, Vol. 15, (A.J. Bard, Ed.). Marcel Dekker, New York (1980), p. 145.
61. A.J. Bard, F.-R.F. Fan and M.V. Mirkin, in: *Electroanalytical Chemistry*, Vol. 18, (A.J. Bard, Ed.). Marcel Dekker, New York (1994), p. 243.
62. J. Izquierdo, J.J. Santana, S. González and R.M. Souto, *Electrochim. Acta* 55 (2010) 8791.
63. J. Izquierdo, J.J. Santana, S. González and R.M. Souto, *Prog. Org. Coat.* 74 (2012) 526.
64. R.M. Souto and G.T. Burstein, *J. Mater. Sci. Mater. Med.* 7 (1996) 337.
65. G.T. Burstein, C. Liu and R.M. Souto, *Biomater.* 26 (2005) 245.
66. G.T. Burstein and R.M. Souto, *Electrochim. Acta* 40 (1995) 1881.
67. R.M. Souto and G.T. Burstein, in: *Materiales y procesos electródicos*, Vol. 1, (F. Vicente, Ed.). INSDE, Valencia (2002), p. 173.
68. D.M. Gordin, E. Delvat, R. Chelariu, G. Ungureanu, M. Besse, D. Laillé and T. Gloriant, *Adv. Eng. Mater.* 10 (2008) 714.